

Supplemental information

**Structural basis for OAS2 regulation
and its antiviral function**

Veronika Merold, Indra Bekere, Stefanie Kretschmer, Adrian F. Schnell, Dorota Kmiec, Rinu Sivarajan, Katja Lammens, Rou Liu, Julia Mergner, Julia Teppert, Maximilian Hirschenberger, Alexander Henrici, Sarah Hammes, Kathrin Buder, Marcus Weitz, Karl Hackmann, Lars M. Koenig, Andreas Pichlmair, Nadine Schwierz, Konstantin M.J. Sparrer, Min Ae Lee-Kirsch, and Carina C. de Oliveira Mann

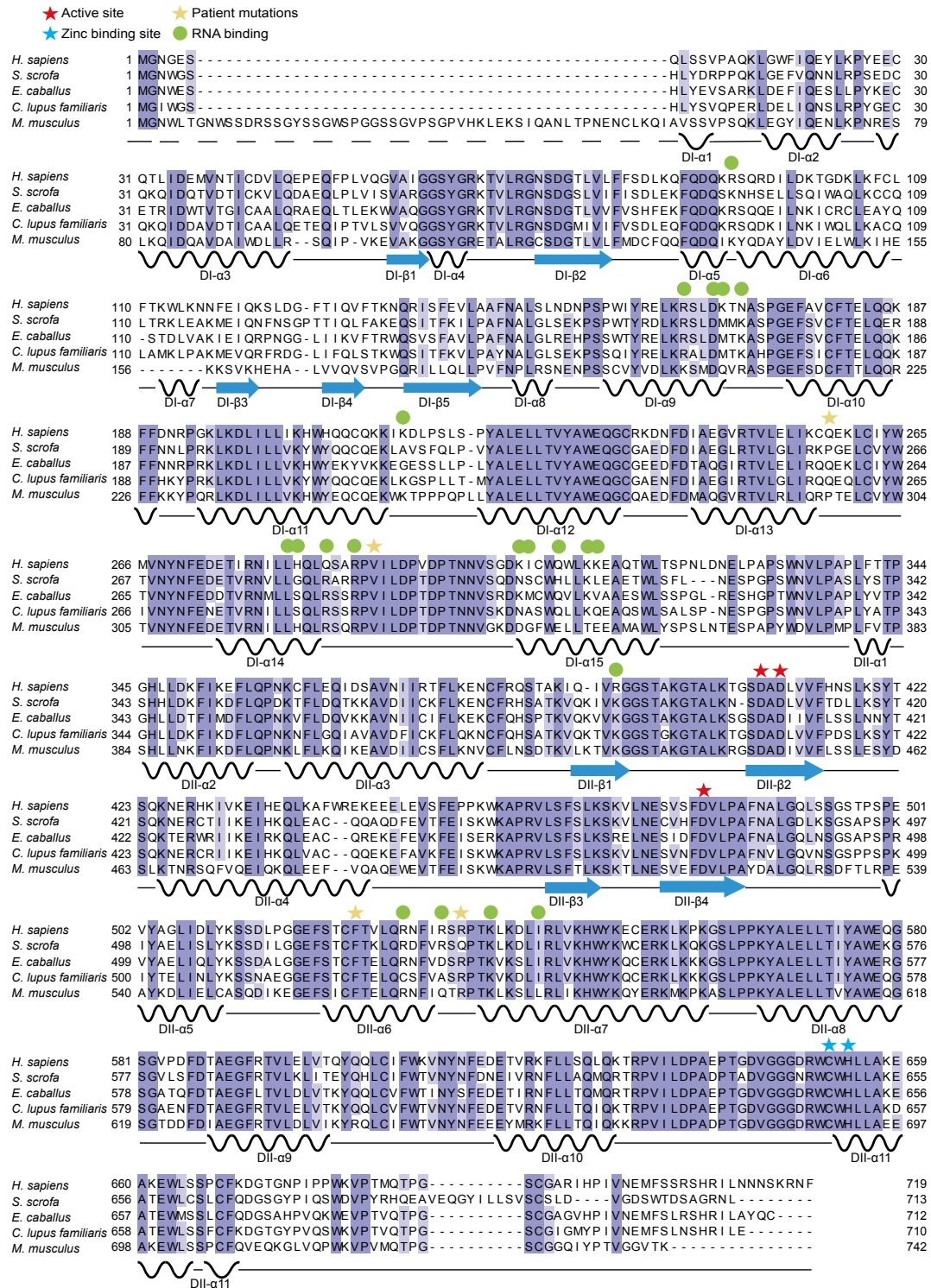


Figure S1. Multiple sequence alignment of OAS2 from selected species. Related to Fig. 1.

Alignment of OAS2 from different species. Active site is depicted with red stars, zinc binding site with blue stars, RNA binding residues with green circles, patient mutations [S1] with yellow stars.

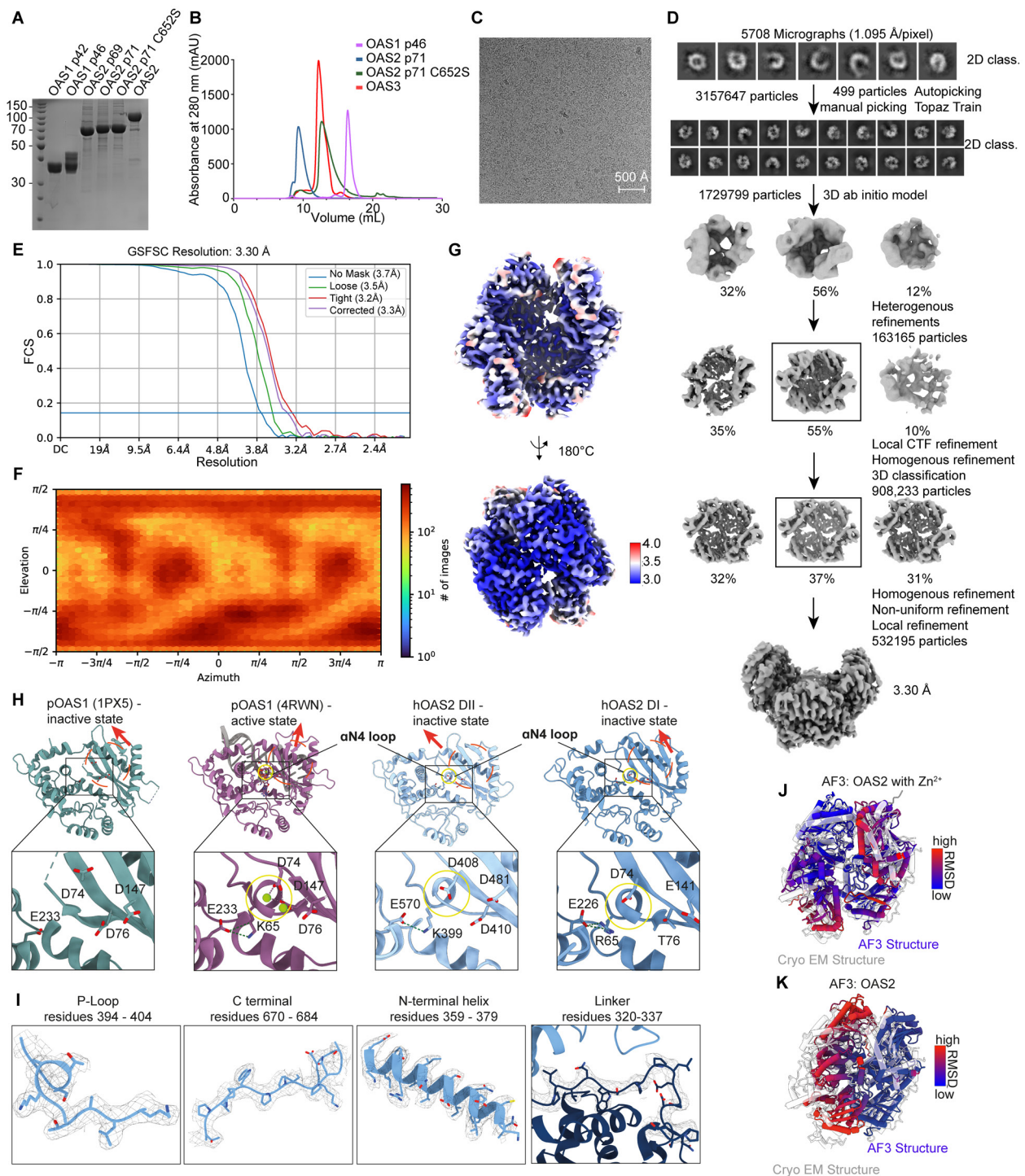


Figure S2. Cryo-em data analysis of OAS2 and structural comparison to OAS1. Related to Fig. 1.

(A) SDS-PAGE of OAS1 p42, OAS1 p46, OAS2 p69, OAS2 p71, OAS2 p71 C652S and OAS3.

(B) Chromatograms of Superdex S200 10/300L of OAS1 p46, OAS2 p71, OAS2 p71 C652S and OAS3.

(C) Representative micrograph of OAS2 apo data set. Scale bar represent 500 Å.

(D) Cryo-em data processing workflow of OAS2 apo data using cryoSPARC v4.5.3.

(E) Map resolution estimated by Gold-standard Fourier shell correlation (GSFSC) with cutoff at 0.143.

(F) Angular distribution dot plot made by CryoSPARC Local refinement job.

(G) Final reconstructed map colored by local resolution. Higher resolution is depicted in blue, lower resolution in red.

(H) Comparison of active site between pOAS1-dsRNA complex (PDB 4RWN, purple), OAS2 DII (light blue), OAS2 DI (dark blue) and pOAS1 apo structure (1PX5). Yellow circles indicate location of P-loop. Red circles depict β -sheets, red arrows indicate orientation of β -sheets.

(I) Electron density for selected areas of cryo-EM model.

(J) Superposition of OAS2 cryo-EM structure (grey) and AF3 predicted dimer with zinc ion colored by RMSD values with low (blue) and high (red) RMSD values.

(K) Superposition of OAS2 cryo-EM structure (grey) and AF3 predicted dimer colored as in (J).

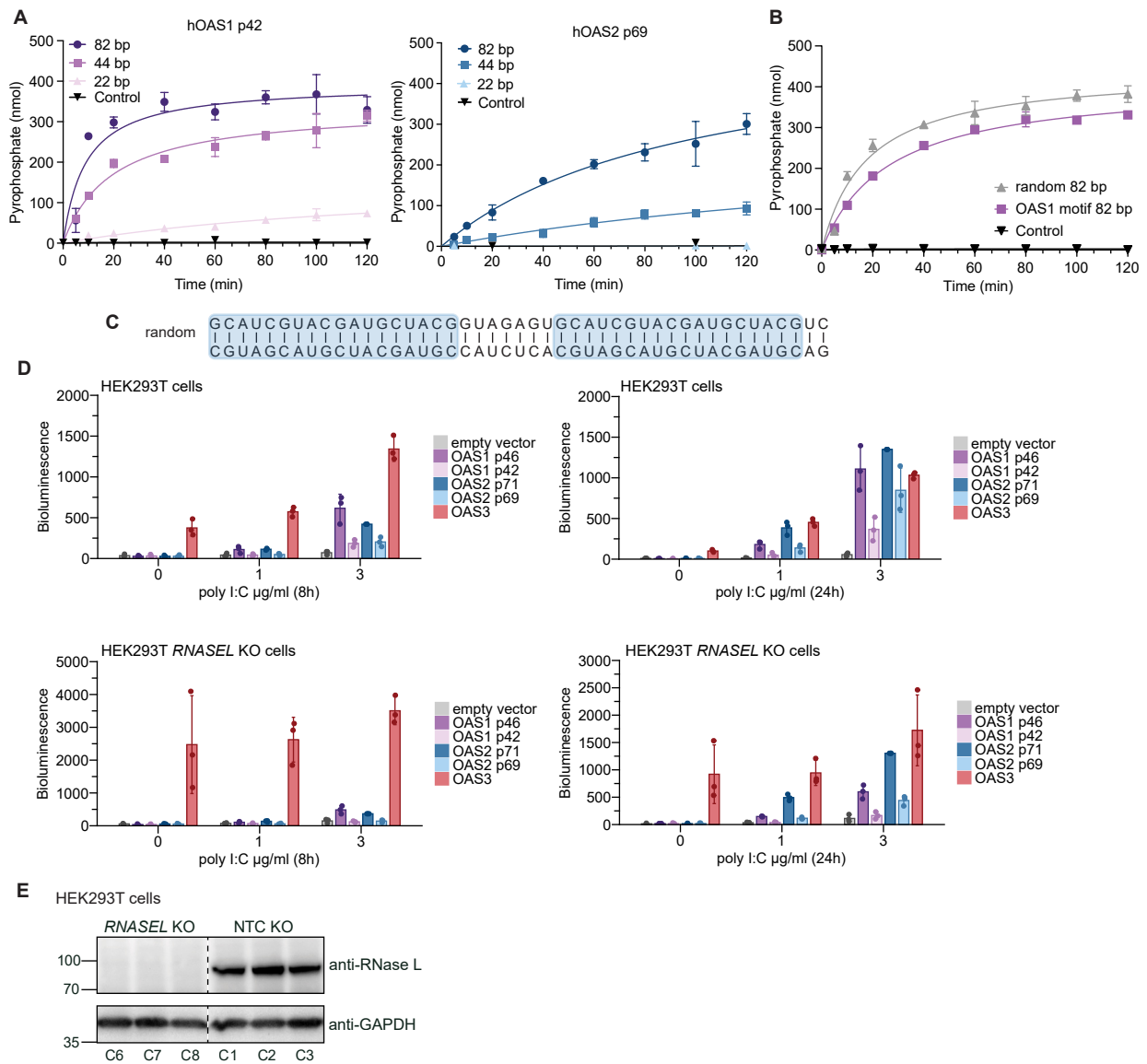


Figure S3. Characterization of OAS activity in-vitro and in cells. Related to Fig. 2.

(A) In-vitro chromogenic activity assay of 200 nM OAS1 p42 and OAS2 p69 with 22 bp, 44 bp, and 82 bp dsRNA (200 nM). dsRNA length is depicted in darker (long RNA) and lighter (short RNA) color (mean \pm SD of $n = 3$).

(B) In-vitro chromogenic activity assay of 100 nM OAS2 p71 with 82 bp random dsRNA and 82 bp OAS1 motif dsRNA (100 nM) (mean \pm SD of $n = 3$).

(C) Sequence of random dsRNA shown in Fig. 2F. Repetitive sequence is depicted in blue.

(D) Analysis of OAS protein activity in cells with 2'-5'OA biosensor for OAS1, OAS2 and OAS3 showing the highest activity for OAS3 even in the absence of poly I:C treatment. HEK293T or HEK293T RNASEL KO cells were transiently transfected with different OAS proteins for 48h followed by transfection of poly I:C. Bioluminescence was measured at 8h and 24h after poly I:C treatment. Bars represent means \pm SD of three independent replicates (dots).

(E) Western blot validation of HEK293T RNASEL and NTC KO monoclonal cells used for 2'-5'OA biosensor assays. The gel was cut to show only the cell lines that were selected for the experiments in the manuscript.

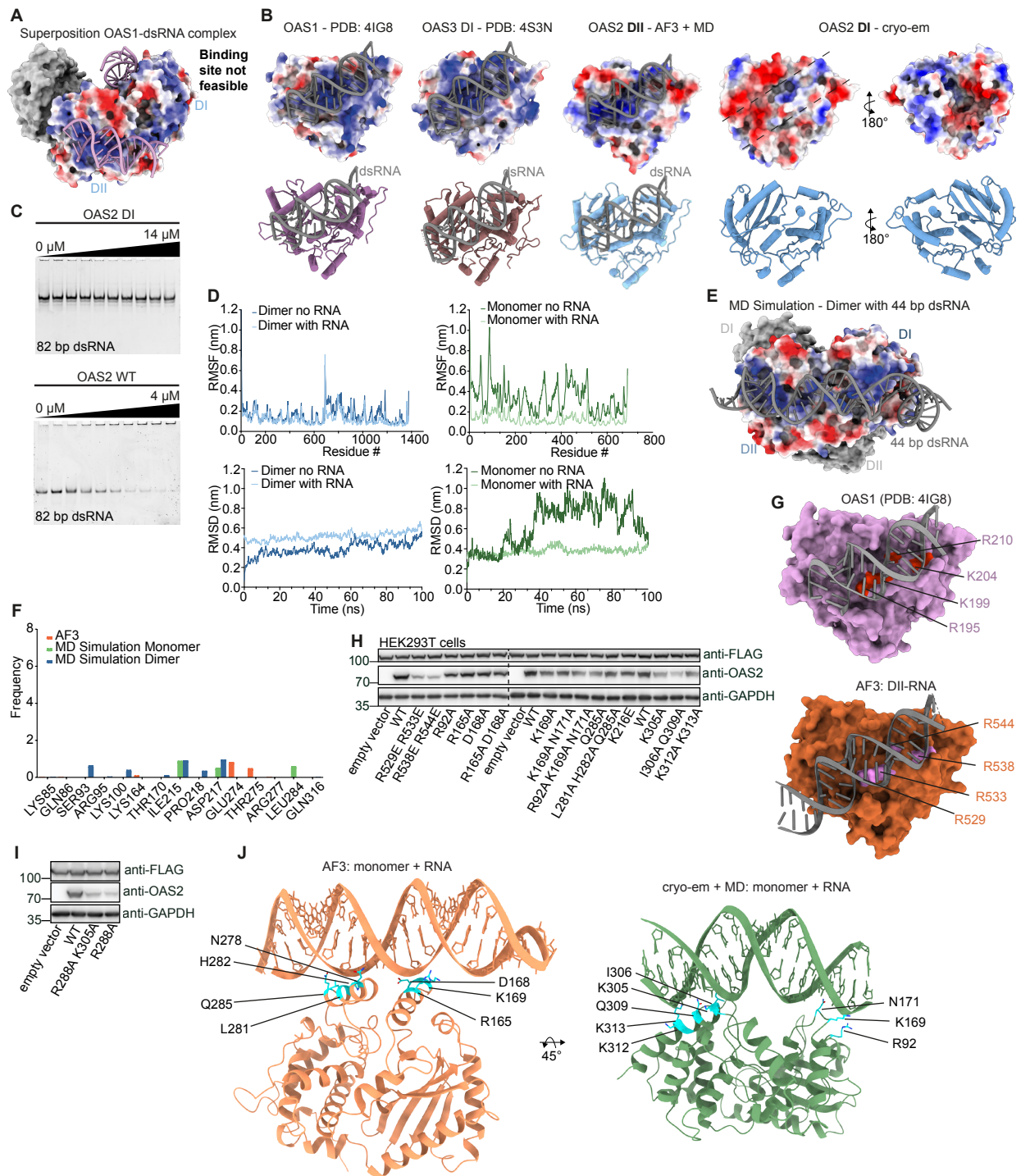


Figure S4. Analysis of a non-canonical RNA binding site of DI. Related to Fig. 3.

(A) Surface representation of OAS2 dimer structure with one monomer depicted as electrostatic surface potential with superposition of crystal structure of OAS1-dsRNA complex (PDB 4IG8, pink) with DI and DII.

(B) Comparison of RNA binding sites of OAS1 (PDB 4IG8), OAS3 DI (PDB 4S3N), OAS2 DI (cryo-em) and DII (AF3 prediction + MD) depicted as electrostatic surface potential and ribbons.

(C) Electrophoretic Mobility Shift Assay of OAS2 DI and OAS2 WT with 82 bp dsRNA. Assays are representative of at least three independent experiments.

(D) RMSF (top) and RMSD (bottom) plots of MD simulations. Simulation data of OAS2 dimer and monomer with RNA are depicted in blue and green, respectively. RMSD was calculated after alignment of backbone atoms, reference: cryo-em structure. For RMSD and RMSF data are shown for monomer and dimer with and without RNA.

(E) Electrostatic surface potential of MD simulation of OAS2 dimer in complex with dsRNA (grey).

(F) Contact frequencies of AF3 predicted monomeric OAS2, MD simulated dimer and monomer with RNA for residues with low frequencies.

(G) Comparison of RNA binding interface of OAS1-RNA complex (4IG8) and AF3-DII.

(H) Western blot validation of OAS2 expression after transient transfection in HEK293T cells for analysis with 2'-5'OA biosensor. Anti-FLAG shows equal expression of FLAG-tagged biosensor and anti-GAPDH was a loading control. The gel image was made out of two gels processed and imaged together.

(I) Western blot analysis of OAS2 wild-type and DI mutants with R288A mutations as in (H).

(J) Close up of OAS2 DI interaction with dsRNA from AF3 and cryo-em + MD.

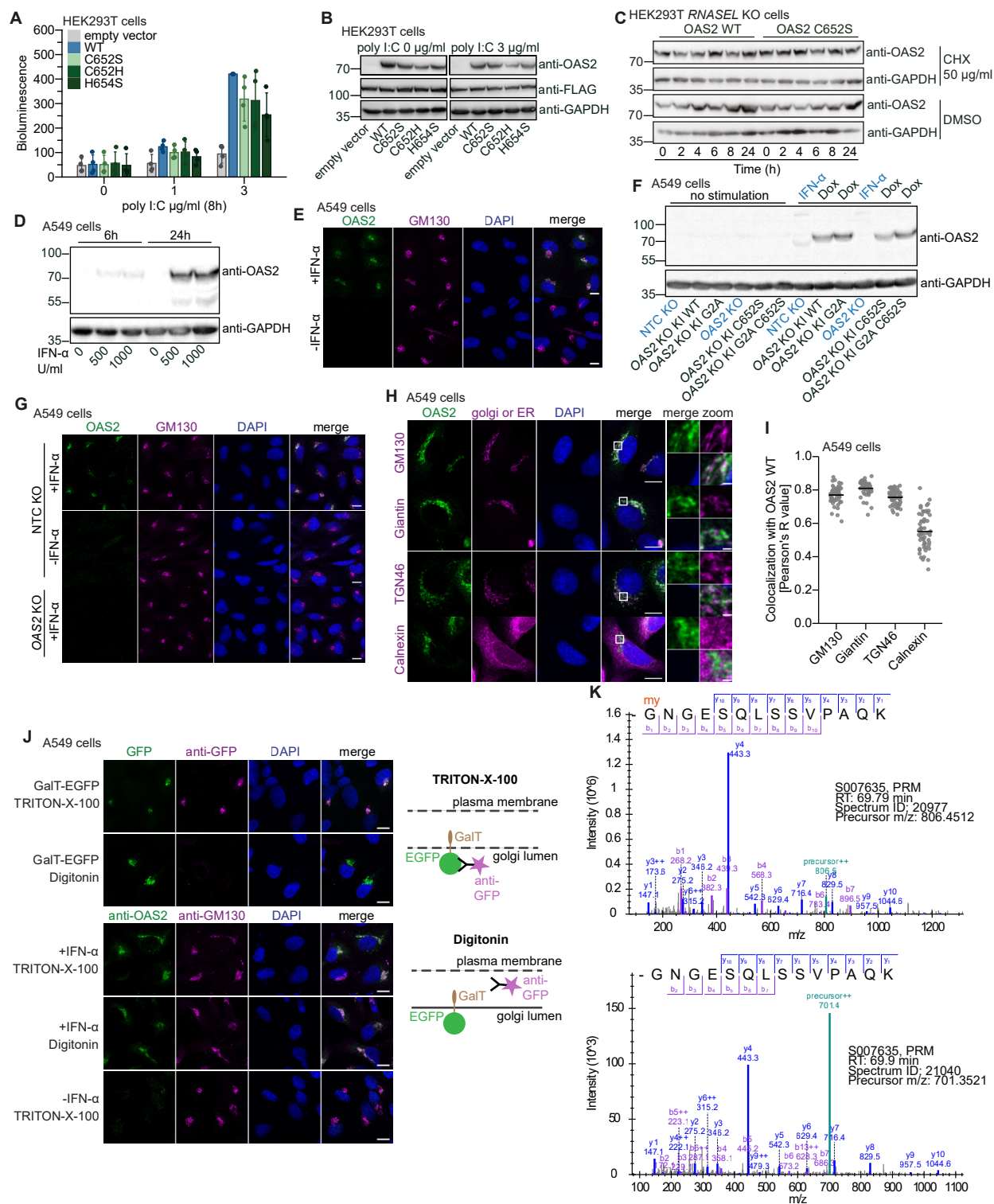


Figure S5. Golgi localization of OAS2 is required for activation. Related to Fig. 4.

(A) Analysis of OAS2 activity in cells with 2'-5'OA biosensor for OAS2 wild-type and monomeric mutants showing higher activity of dimeric wild-type than the monomeric mutants. HEK293T were transiently transfected with different OAS2 constructs for 48h followed by treatment with poly I:C. Bioluminescence was measured at 8h after poly I:C transfection. Bars represent means \pm SD of four independent replicates (dots).

(B) Western blot validation of OAS2 expression after transient transfection in HEK293T cells for activity measurements with 2'-5'OA biosensor. Anti-FLAG shows equal expression of FLAG-tagged biosensor and anti-GAPDH was a loading control.

(C) Western blot analysis of OAS2 WT and OAS2 C652S stability after cycloheximide (CHX) treatment. HEK293T *RNASEL* KO cells were transiently transfected with OAS2 constructs for 24h followed by treatment with 50 $\mu\text{g/ml}$ CHX or DMSO for indicated time points.

(D) Western blot validation of endogenous OAS2 expression in A549 cells after stimulation with 500 U/ml or 1000 U/ml IFN- α for 6h and 24h. GAPDH is shown as a loading control.

(E) Immunofluorescence confocal microscopy of OAS2 localization in A549 cells after stimulation with 500 U/ml IFN- α . Staining was performed for OAS2 (green), golgi marker GM130 (magenta) and DAPI (blue). Scale bars represent 10 μm .

(F) Western blot validation of OAS2 expression in A549-OAS2 KO cells reconstituted with doxycycline-inducible OAS2 constructs. Cells were stimulated with 500 U/ml IFN- α or 1 μ g/ml doxycycline for 24h. GAPDH is shown as a loading control.

(G) Immunofluorescence microscopy as in (E) in A549 OAS2 KO and NTC KO cells.

(H) Immunofluorescence Airyscan microscopy of endogenous OAS2 localization in A549 cells after stimulation with 500 U/ml IFN- α for 24h. Staining was performed for OAS2 (green), DAPI (blue) and ER or golgi markers (magenta): GM130 (cis-golgi), Giantin (medial-golgi), TNG46 (trans-golgi network) and Calnexin (ER). Scale bars represent 10 μ m and 1 μ m for zoom in.

(I) Quantification of colocalization of OAS2 and golgi or ER markers from (H) based on Pearson correlation. Means are shown from measurements in individual cells (dots).

(J) Analysis of OAS2 cytosolic or golgi lumen localization by immunofluorescence Airyscan microscopy and digitonin or TRITON-X-100 permeabilization. Top: A549 cells were transfected with GalT-EGFP-expressing plasmid, producing a fusion protein with EGFP facing the golgi lumen. EGFP fluorescence (green) is visible both by permeabilization with TRITON-X-100 (permeabilizes plasma membrane and golgi membrane) and digitonin (permeabilizes plasma membrane but not golgi membrane). Staining by anti-GFP antibody (magenta) is visible only after TRITON-X-100 permeabilization. Bottom: A549 cells were treated with 500 U/ml IFN- α for 24h and OAS2 (green) and GM130 (magenta) staining was observed both after TRITON-X-100 and digitonin permeabilization, indicating that OAS2 is facing cytosol and not golgi lumen at the golgi membrane. Scale bar represent 10 μ m.

(K) Representative annotated ms/ms spectra for the myristoylated (top) and unmodified (bottom)

GNGESQLSSVPAQK tryptic peptide of OAS2. Fragment ions of y-ion series (blue) and b-ion series (violet) are shown for each peptide.

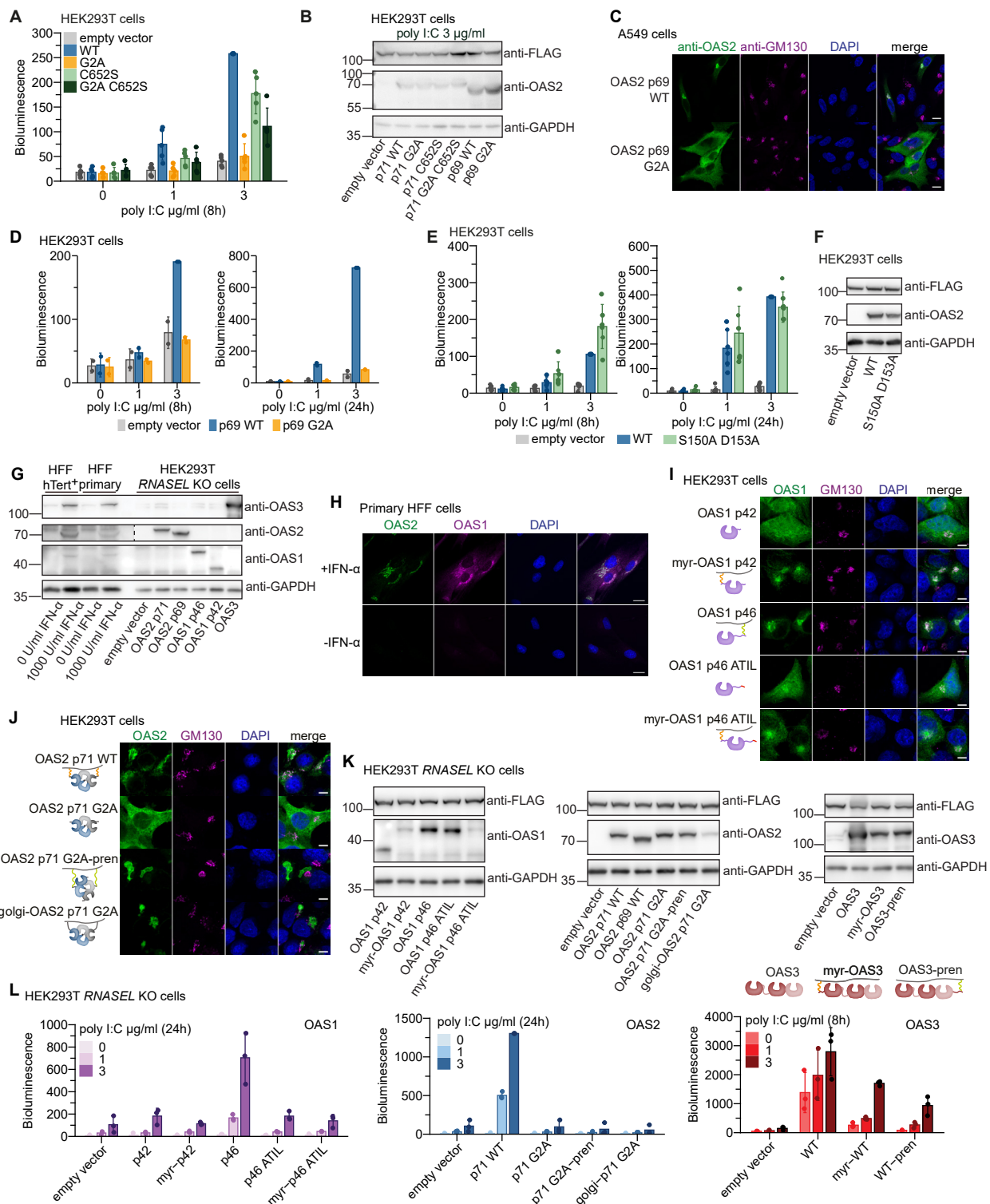


Figure S6. Subcellular localization of OAS proteins. Related to Fig. 4.

(A) Analysis of OAS2 activity in cells with 2'-5'OA biosensor for OAS2 wild-type and mutants with different localization. HEK293T were transiently transfected with different OAS2 constructs for 48h followed by treatment with poly I:C. Bioluminescence was measured at 8h after poly I:C transfection. Bars represent means \pm SD of five independent replicates (dots).

(B) Western blot validation of OAS2 expression after transient transfection in HEK293T cells for activity measurements with 2'-5'OA biosensor. Anti-FLAG shows equal expression of FLAG-tagged biosensor and anti-GAPDH was a loading control.

(C) Immunofluorescence Airyscan microscopy of A549 cells transfected with OAS2 p69 WT or OAS2 p69 G2A and stained for OAS2 (green), GM130 (magenta) or DAPI (blue). Scale bars represent 10 μm .

(D) Analysis of OAS2 activity in cells with 2'-5'OA biosensor for OAS2 p69 WT and OAS2 p69 G2A as in (A) showing loss of activity when myristoylation is disrupted. Bars represent means \pm SD of two independent replicates (dots).

(E) Analysis of OAS2 activity in cells as in (A) after 8h and 24h after poly I:C transfection for OAS2 wild-type and DI-DII interaction mutant S150A D153A showing higher activity when dimeric OAS2 wild-type conformation is destabilized in S150A D153A mutant. Bars represent means \pm SD of six independent replicates (dots).

(F) Western blot validation of OAS2 expression as in (B).

(G) Western blot analysis of OAS protein expression in BJ primary and hTERT⁺ HFF cells after stimulation with 1000U/ml IFN- α for 24h. Cell lysates from transient transfection of HEK293T *RNASEL* KO cells were loaded in parallel as a reference. GAPDH is shown as loading control. The gel was cut because images with different exposures for anti-OAS2 were used for the figure.

(H) Immunofluorescence Airyscan microscopy of OAS2 and OAS1 localization in BJ primary HFF cells after stimulation with 1000U/ml IFN- α for 24h. Staining was performed for OAS2 (green), OAS1 (magenta) and DAPI (blue). Scale bars represent 20 μ m.

(I) Immunofluorescence Airyscan microscopy of OAS1 isoforms and chimeras in transiently transfected HEK293T cells. Staining was performed for OAS1 (green), golgi marker GM130 (magenta) and DAPI (blue). Scale bars represent 10 μ m.

(J) As in (I) but for OAS2. Golgi-OAS2 construct was designed by adding 10 amino acids to the OAS2 G2A N-terminus as shown in [S2] to target OAS2 G2A to the Golgi.

(K) Western blot validation for expression of OAS protein isoforms and chimeras in HEK293T *RNASEL* KO used for activity measurements in cells with 2'-5'OA biosensor in (L). Anti-FLAG shows equal expression of FLAG-tagged biosensor and anti-GAPDH was a loading control.

(L) Analysis of OAS2 activity in cells with 2'-5'OA biosensor for OAS protein isoforms and their chimeras with prenylation or myristoylation. Assay shows that OAS2 and OAS1 p46 are active only when myristoylated and prenylated, respectively, whereas membrane targeting reduces the activity of OAS3. HEK293T were transiently transfected with different OAS constructs for 48h followed by transfection of poly I:C. Bioluminescence was measured at 24h (OAS1, OAS2) or 8h (OAS3) after poly I:C transfection. Bars represent means \pm SD of three independent replicates (dots).

“myr” indicates N-terminal fusion with myristoylation motif from OAS2, while “pren” indicates C-terminal fusion with prenylation motif from OAS1 p46.

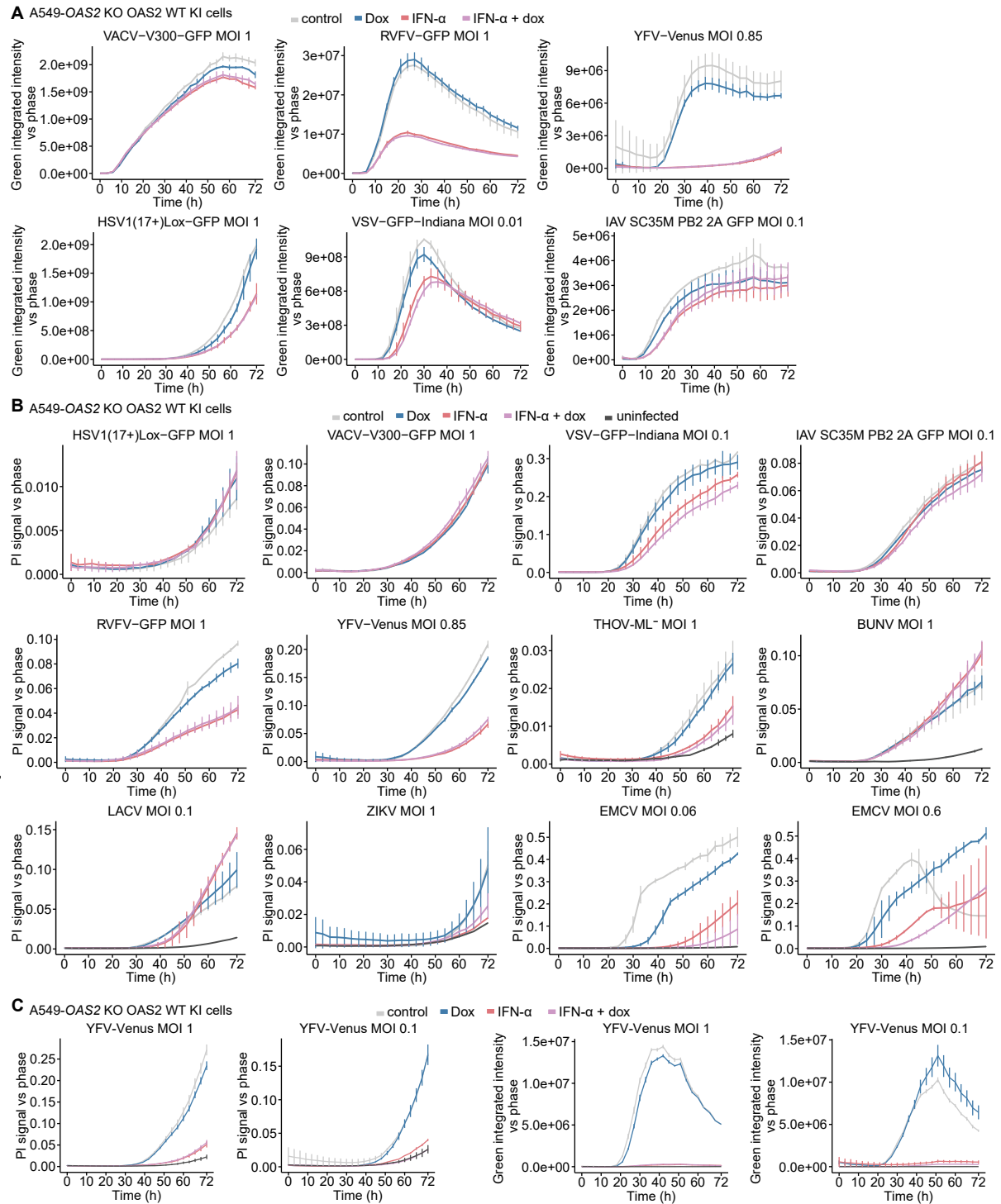


Figure S7. Virus infection screen. Related to Fig. 5.

(A) Virus replication in A549 OAS2 KO cells reconstituted with doxycycline-inducible OAS2 WT after infection with different GFP-reporter viruses as described in Fig 5A. Virus replication was quantified as GFP integrated intensity versus cell confluency.

(B) Cell death analysis as in (A). Cell death was quantified as area of propidium iodide (PI) signal versus cell confluency.

(C) Cell death analysis and virus replication analysis for YFV-Venus. Cell death was quantified as area of propidium iodide signal versus cell confluency and virus replication was quantified as green integrated intensity versus cell confluency.

In (A), (B) and (C) bars represent mean from two technical replicates. Panel (C) is representative of at least three independent experiments.

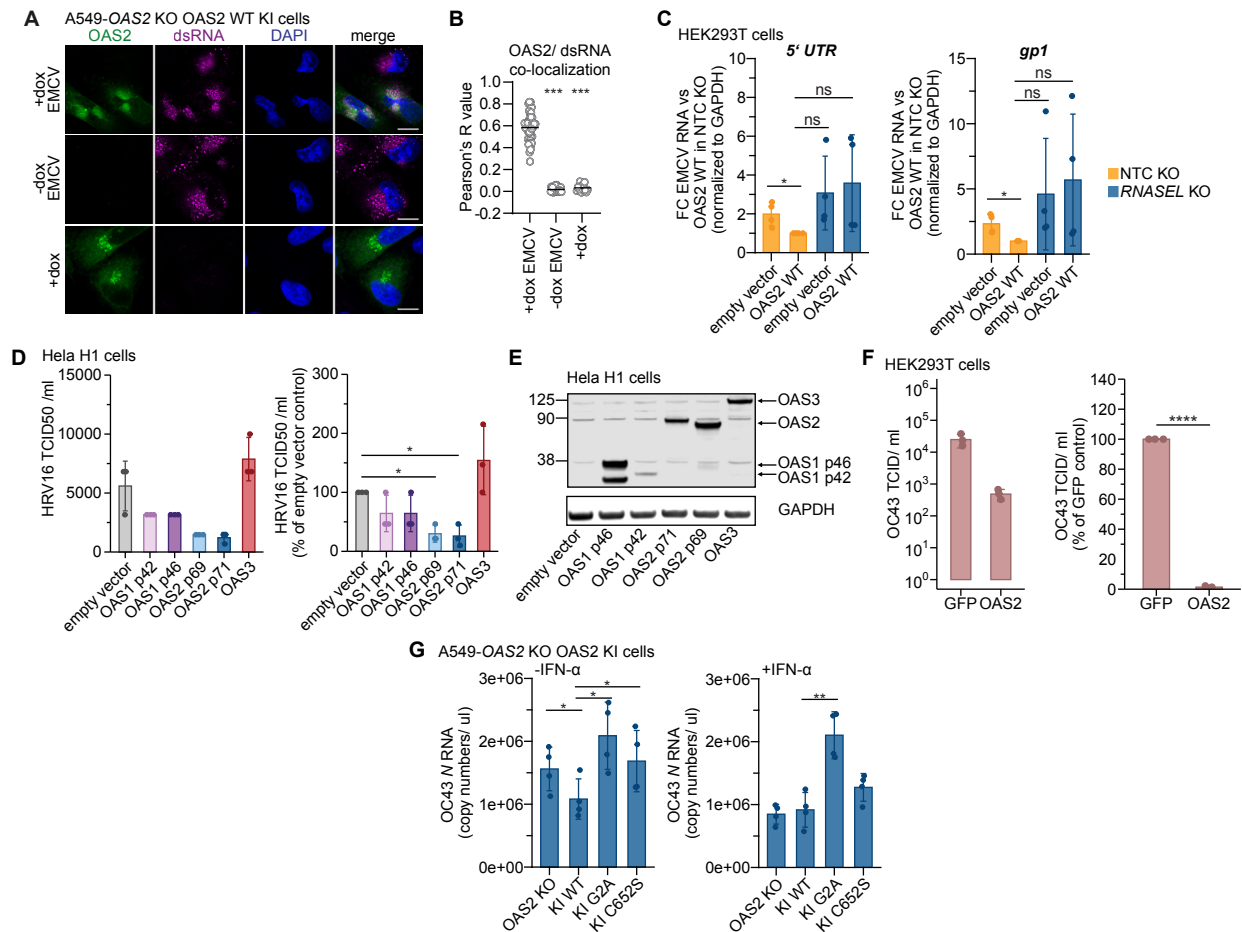


Figure S8. Analysis of viruses restricted by OAS2. Related to Fig. 5.

(A) Immunofluorescence Airyscan microscopy of OAS2 localization during EMCV infection in A549 OAS2 KO cells reconstituted with doxycycline-inducible OAS2 WT. Staining was performed for OAS2 (green), dsRNA (magenta) and DAPI (blue). Scale bars represent 10 μ m.

(B) Quantification of colocalization of OAS2 and dsRNA markers from (A) based on Pearson correlation. Lines represent means from measurements of individual cells (dots). Statistical analysis was performed with Student's T-test with Welch's correction. *** $p \leq 0.001$.

(C) RT-qPCR analysis of intracellular EMCV RNA levels for 5' UTR and gp1 in HEK293T monoclonal RNASEL KO and NTC KO cells. Cells were transfected with OAS2 WT or empty vector control for 24h followed by EMCV infection for 20h with MOI of 1. Bars represent means \pm SD of three independent replicates (dots). Paired T-test: ns $p > 0.05$, * $p \leq 0.05$.

(D) HRV16 virus titers measured by plaque assay in Hela H1 cells transiently transfected with indicated OAS proteins as TCID50/ml (left) and percent TCID50/ml of empty vector control (right). Bars show means \pm SD from three independent replicates. Paired T-test: * $p \leq 0.05$.

(E) Western blot validation of OAS protein expression in Hela H1 cells after transient transfection.

(F) As in (E) but for OC43 virus titers measured by plaque assay in HEK293T cells transiently transfected with GFP (control) or OAS2 p69 WT. Paired T-test: **** $p \leq 0.0001$.

(G) RT-qPCR analysis of OC43 RNA levels in culture supernatants in A549 OAS2 KO cells reconstituted with doxycycline-inducible OAS2 constructs. Cells were treated with 1 μ g/ml doxycycline with (right) or without (left) 500U/ml IFN- α for 24h followed by infection with OC43 for 72h. Bars represent means of four independent biological replicates (dots). Statistical significance was calculated using paired T-test. * $p \leq 0.05$, ** $p \leq 0.001$.

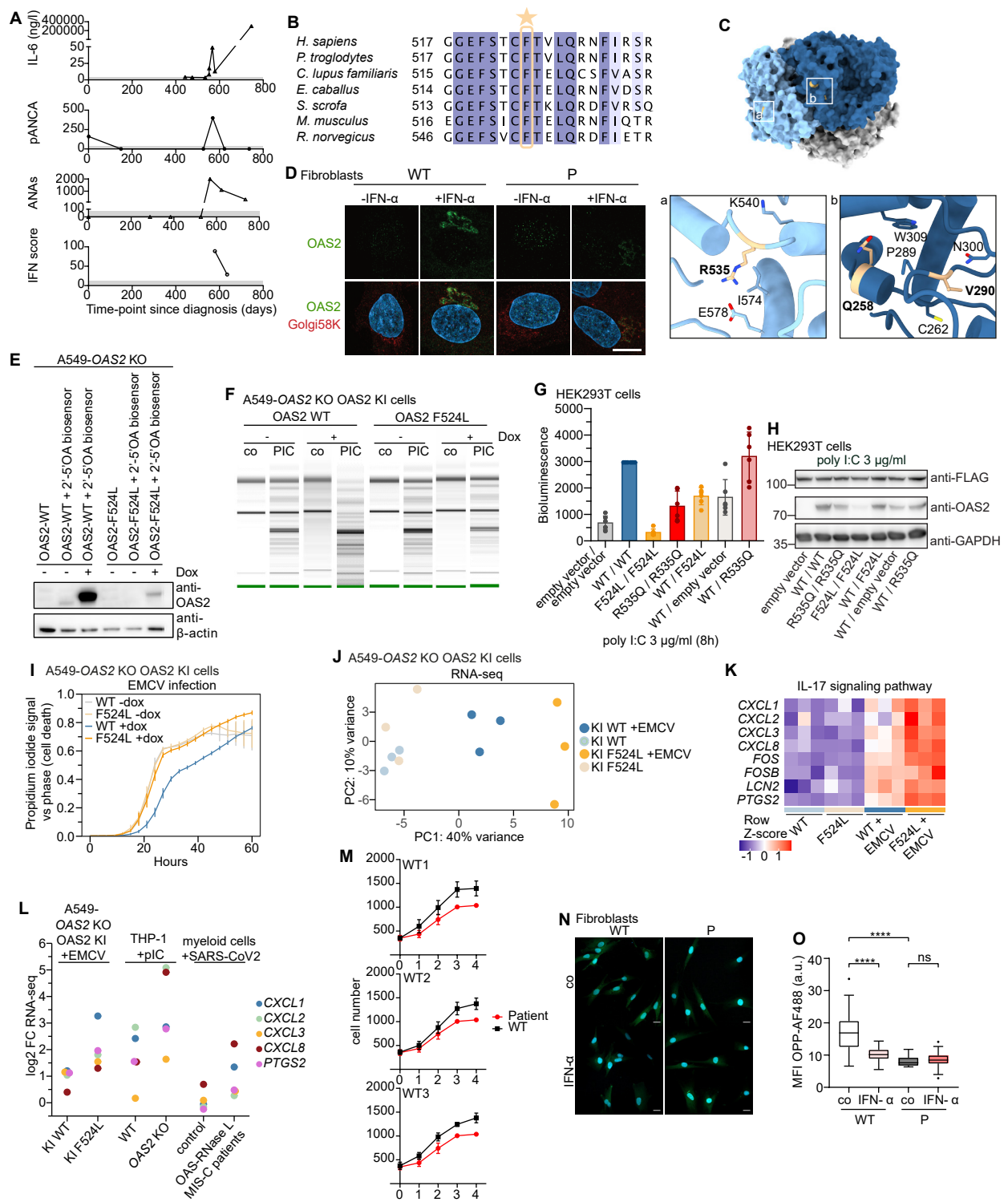


Figure S9. Characterization of effects of OAS2 F524L. Related to Fig. 6.

(A) Patient's serum levels of interleukin-6 (IL-6), perinuclear anti-neutrophil cytoplasmic antibodies (pANCA), and antinuclear antibodies (ANA). The IFN score was calculated as previously described [S3]. Grey bars indicate normal ranges.

(B) Multiple sequence alignment across different species indicating high conservation of the F524 (yellow star) of the human OAS2 protein.

(C) Surface view of OAS2 depicted in two protomers, blue and grey. DI and DII are indicated in darker and lighter color, respectively. Patient mutations are indicated in yellow [S1]. Close ups show show interaction of residues R535 (a) and Q258 and V290 (b).

(D) Immunofluorescence staining for OAS2 and Golgi 58K in patient and wild-type fibroblasts. Scale bar = 10 μm.

(E) Western blot validation of OAS2 expression in A549 OAS2 KO cells reconstituted with doxycycline-inducible OAS2 constructs. Cells were stimulated with 1 μg/ml doxycycline for 24h and transfected with V6 RNase L WT 2'-5'OA biosensor. β-actin is shown as a loading control.

(F) RNA chip analysis of total RNA cleavage in A549 OAS2 KO cells reconstituted with either doxycycline-inducible OAS2 WT or OAS2 F524L untreated or treated with 2 μg/ml poly(I:C) for 24 h.

(G) Analysis of OAS2 activity in cells with 2'-5'OA biosensor for OAS2 wild-type and patient mutations F524L and R535Q or 1:1 mixes showing loss of activity for the F524L mutant and strongly reduced activity of WT / F524L mix mimicking heterozygous situation. HEK293T were transiently transfected with different OAS2 constructs for 48h followed by transfection of poly I:C. Bioluminescence was measured at 8h after poly I:C treatment. Bars show means \pm SD from six independent replicates.

(H) Western blot validation of OAS2 protein expression from cellular activity assays with 2'-5'OA biosensor. Anti-FLAG shows equal expression of FLAG-tagged biosensor.

(I) Cell death analysis with propidium iodide staining in A549 OAS2 KO cells reconstituted with doxycycline-inducible OAS2 WT or OAS2 F524L and infected with EMCV (MOI 0.6) over time course of 60h. Data represent mean from two technical replicates and are representative of at least three independent experiments.

(J) PCA plot from RNA-seq showing clustering based on normalized counts of 1000 most variable genes.

(K) Heatmap of RNA-seq normalized counts for genes belonging to KEGG pathway "IL-17 signaling pathway".

(L) Log2 fold changes for inflammatory genes from (K) in A549 cells and publicly available data sets from in THP-1 cells and myeloid cells from MIS-C patients with OAS-RNase L pathway mutations [S1].

(M) Proliferation curve of wild-type (WT) and patient-derived fibroblasts (P) over 4 days. Data are mean \pm SEM pooled from technical replicates.

(N) Representative images of the OPP Alexa Fluor 488 protein synthesis analysis in untreated or IFN- α -stimulated fibroblasts from patient and healthy control, scale bar = 20 μ m.

(O) Quantification of mean fluorescence intensity (MFI) of Alexa Fluor 488-OPP in cells shown in (N). n = 26-55 cells. Box plots: center line, median; box, interquartile range; whiskers, 1.5x interquartile range. Two-way ANOVA with Sidak's multiple comparisons test. **** p \leq 0.0001.

Supplemental References

- [S1] Lee, D., Le Pen, J., Yatim, A., Dong, B., Aquino, Y., Ogishi, M., Pescarmona, R., Talouarn, E., Rinchai, D., Zhang, P., et al. (2022). Inborn errors of OAS–RNase L in SARS-CoV-2–related multisystem inflammatory syndrome in children. *Science*, eabo3627. 10.1126/science.abo3627.
- [S2] Navarro, A.P., and Cheeseman, I.M. (2022). Identification of a Golgi-localized peptide reveals a minimal Golgi-targeting motif. *Mol Biol Cell* 33, ar110. 10.1091/mbc.E22-03-0091.
- [S3] Wolf, C., Brück, N., Koss, S., Griep, C., Kirschfink, M., Palm-Beden, K., Fang, M., Röber, N., Winkler, S., Berner, R., et al. (2020). Janus kinase inhibition in complement component 1 deficiency. *J Allergy Clin Immunol* 146, 1439-1442.e1435. <https://doi.org/10.1016/j.jaci.2020.04.002>.

Data S1

Extended case report

The female patient was born at term as the first child of non-consanguineous healthy parents of Caucasian descent after an uneventful pregnancy. Her birth weight and length were normal and she developed normally. At the age of 4 years and 1 month, she presented with progressive fatigue since four weeks, epistaxis since two weeks, and hemochezia since one week. The pediatrician referred the child to the hospital because of a hemoglobin of 6.1 g/dl [11.1-14.3 g/dl]. On admission, acute-on-chronic renal failure was diagnosed with creatinine 4.4 mg/dl [0.2-0.6 mg/dl], urea 143 mg/dl [10-35 mg/dl], cystatin C 3.6 mg/dl [0.64-1.03 mg/l], metabolic acidosis (pH 7.29, base excess -9.8 mmol, HCO_3^- 17 mmol/l), and hyperkalemia 6.6 mmol/l [3.4-4.7 mmol/l]. Urine analysis showed microhematuria and nephrotic-range proteinuria (urine-protein/creatinine ratio 5590 mg/g). Infections with Hantavirus, CMV, EBV, HBV, HAV, HCV, HIV, streptococci, enterohemorrhagic *E. coli*, *Campylobacter*, *Salmonella*, and *Shigella* were excluded. She tested positive for perinuclear anti-neutrophil cytoplasmic antibodies (p-ANCA; 1:160 [$<1:80$]), antibodies to myeloperoxidase (MPO; 46 U/ml [<20 U/ml, and antinuclear antibodies (ANA 1:320 to 1:2000 [$<1:80$])) (**Fig. 6A, SI Fig. 9A**). Renal ultrasound showed mildly hyperechogenic kidneys. Renal biopsy showed severe glomerulosclerosis (10 out of 18) with fresh and older areas of a proliferative extracapillary glomerulonephritis with two cellular and four fibrocellular crescents in eight non-scarred glomeruli and segmental necrotizing vasculitis of an interlobular artery, consistent with ANCA-associated vasculitis. There was also evidence of severe tubular epithelial damage with tubular atrophy and interstitial fibrosis, and chronic interstitial inflammation (**Fig 6B, Suppl Figure A, B**). Based on these findings, a diagnosis of MPO-ANCA-associated vasculitis with end-stage renal disease was made. Vasculitis was treated with i.v. methylprednisolone pulses (500 mg/m² body surface area/day i.v. for 5 days), followed by prednisolone tapering (2.2-0.2 mg/kg body weight for 8 months), rituximab (2 doses á 375 mg/m² body surface area) and azathioprine (2.8-1.5 mg/kg body weight/day for 3 months, stopped due to leucopenia). End-stage renal disease was treated by intermittent hemodialysis initially and switched to peritoneal dialysis. She developed severe hypertension and was treated with metoprolol, amlodipine, ramipril, and dihydralazine. The patient was also given vitamin D, calcitriol, calcium carbonate, azathioprine, potassium- and phosphate-reduced diet, erythropoietin, iron, and one blood transfusion. Hypertrophic

osteoarthropathy was diagnosed 8 months after disease manifestation (**Suppl Figure C**). Because of increasing pANCA and MPO antibodies 11 months after disease manifestation, prednisolone was started again (0.6-0.1 mg/kg body weight/day). Growth retardation was attributed to an eating disorder, long-term corticosteroid therapy, and end-stage renal disease.

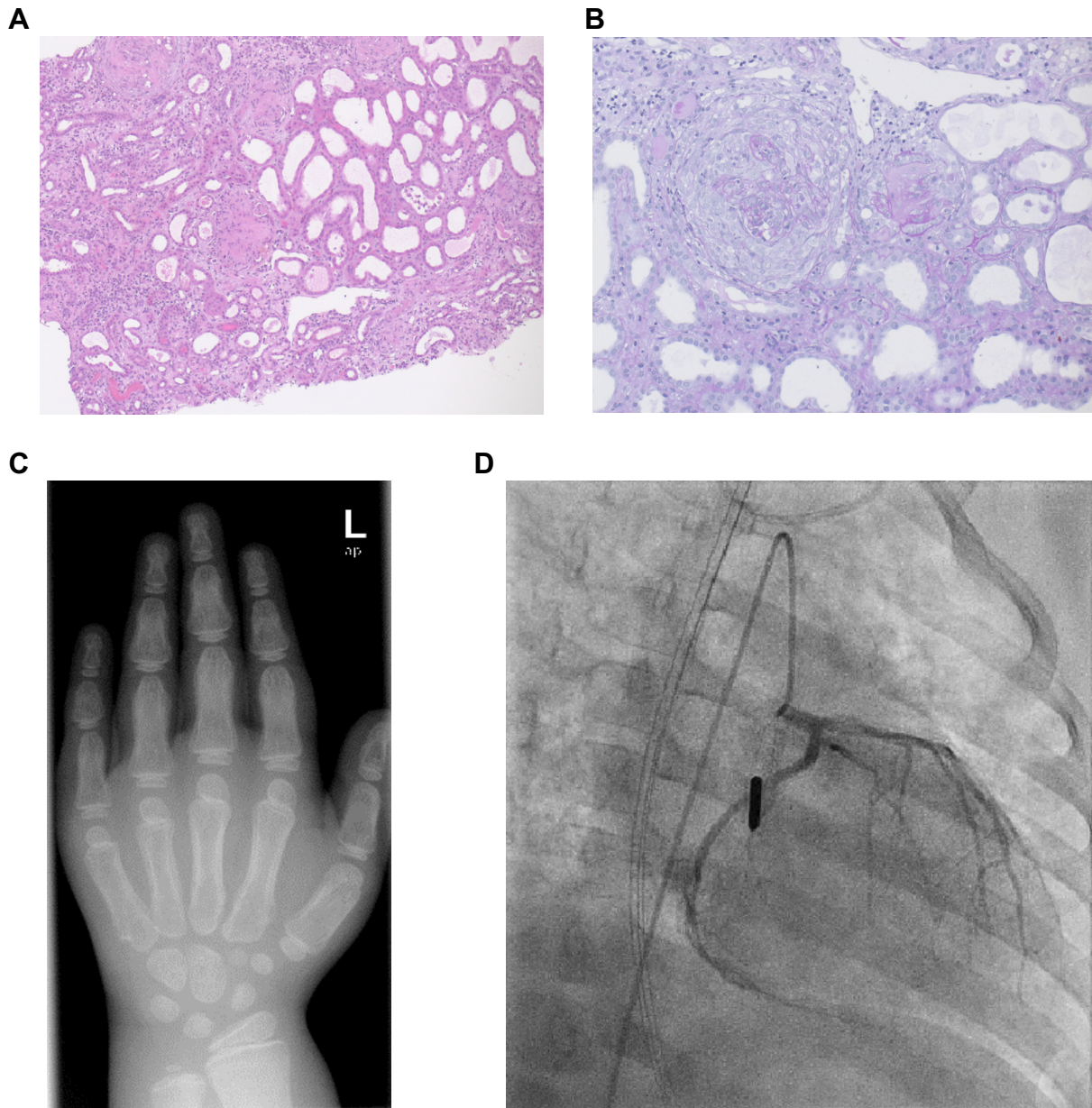
At the age of 5 years and 2 months, the patient was admitted to the hospital with fever and suspected bronchopneumonia. A chest x-ray showed bilateral infiltrations in the central lung areas extending to the lower fields. Tests for mycoplasma and SARS-Cov2 were negative. She was treated with ampicillin/sulbactam and discharged after five days. 10 days later, the patient presented with chest pain and dyspnea due to acute coronary syndrome with ST elevation myocardial infarction. Cardiac catheterization revealed non-perfusion of the anterior ramus interventricularis of the left coronary artery (**Suppl Figure D**). The patient was started on dual platelet aggregation inhibition and lysis therapy. Over the next two weeks, she experienced episodes of tachycardia arrhythmia and ST elevations, a transfusion-dependent lower gastrointestinal bleeding, and hypertensive crises due to massive intracerebral hemorrhage with high intracranial pressure requiring craniectomy and deep sedation. Brain magnetic resonance imaging showed multiple bilateral ischemic areas in the occipital, left thalamus, and right temporal regions. A progressive increase in gamma-glutamyltransferase to 5900 U/l [<25 U/l] suggested primary sclerosing cholangitis as part of the vasculitis. After extubation, the patient developed hemiparesis of the right lower limb.

During acute coronary syndrome, the patient was found to have elevated inflammatory markers (**Fig 6A, SI Fig. 9A**). Despite negative investigations for infections including Influenza A/B, RSV, SARS-Cov2, Rotavirus, Adenovirus, Norovirus, HSV, VZV, and bacterial and fungal infections in tracheal secretions, blood, cerebrospinal fluid, and stool, she was treated with antibiotic therapy with piperacillin/tazobactam, tobramycin, and clindamycin. She was started on immunosuppressive therapy with mycophenolate mofetil (760 mg/m² body surface area/day), one additional methylprednisolone pulse, and the prednisolone dose was again increased (up to 2 mg/kg body weight/day). She was also given immunomodulatory therapy with daily anakinra applications (for 3 weeks), one i.v. immunoglobulin administration, and infliximab (every four weeks) due to persistent inflammatory signs with elevated levels of C-reactive protein (CRP) up to

28.81 mg/dl [<0.5 mg/dl] and soluble IL-2 receptor (sIL-2R) up to 5808 U/ml [158-613 U/ml]).

At the age of 5 years and 7 months, she was readmitted for percutaneous endoscopic gastrostomy because of deterioration in her general condition and eating disorder with associated trichophagia and trichobezoar. During this hospitalization, the child developed epileptic seizures which were treated with midazolam and levetiracetam. She also developed signs of pulmonary edema with tachydyspnea and oxygen requirements, accompanied by elevated inflammatory markers (CRP 4.3 mg/dl [<0.5 mg/dl]; sIL-2R >6000 U/l [158-613 U/ml]). She was treated with methylprednisolone pulse therapy, midazolam and levetiracetam. Throat swabs were negative for Influenza/B virus, RSV, and SARS-Cov2. Due to progressive inflammatory signs, she was started on methylprednisolone pulses and prednisolone escalation, and switched from infliximab to anakinra (up to 5 mg/kg). Further investigations for autoinflammation revealed normal adenosine deaminase 2 activity and elevated interferon (IFN) signatures (IFN score 88.96 and 28.74 [<12.49]).

At the age of 6 years and 1 month, the child had an acute episode of chest pain, fatigue, and tachydyspnea. An ECG showed ST elevation and a cardiac echogram showed a massive decrease in cardiac contractility. Due to circulatory failure with hypotension, she was intubated and treated with catecholamines, hydrocortisone, and vasopressin. This was accompanied by a massive increase in interleukin-6 (IL-6 300,000 ng/l [<4 ng/l]), CRP 2.3 mg/dl [<0.5 mg/dl]) and leukopenia. Antibiotic therapy with meropenem and vancomycin was started. A cytokine storm due to bacterial sepsis was suspected as the cause of the circulatory failure, and she was also treated with methylprednisolone, anakinra, and immunoglobulins. However, myocardial function and circulation could not be stabilized due to refractory hypotension and inadequate organ perfusion, and the child died only few hours after admission to intensive care.



Supplementary Figure. Renal histology, hand x-ray and coronary angiography.

A, B. Histopathological findings of the renal biopsy showing areas of a proliferative extracapillary glomerulonephritis with cellular crescents, necrotizing vasculitis of an interlobular artery, along with tubular epithelial damage with tubular atrophy and interstitial fibrosis, as well as interstitial inflammation, consistent with ANCA-associated vasculitis. Hematoxylin and eosin stain, 10x magnification (A), periodic acid–Schiff stain, 20x magnification (B). **C.** X-ray of the left hand at the age of 5 years and 9 months showing osteopenic bone with double contours of the metacarpophalangeal and phalangeal periosteum, consistent with hypertrophic osteoarthropathy. **D.** Coronary angiography showing underperfusion of the peripheral segment of the left coronary artery, particularly the anterior interventricular ramus.